SELF-SUPERVISED TEMPORAL SUPER RESOLUTION OF ENERGY DATA USING GENERATIVE ADVERSARIAL TRANSFORMERS

Xuanhao Mu, Gökhan Demirel, Yuzhe Zhang, Jianlei Liu, Thorsten Schlachter and Veit Hagenmeyer
Institute for Automation and Applied Informatics (IAI)
Karlsruhe Institute of Technology
76344 Eggenstein-Leopoldshafen, Germany
xuanhao.mu@kit.edu goekhan.demirel@kit.edu yuzhe.zhang@student.kit.edu
jianlei.liu@kit.edu thorsten.schlachter@kit.edu veit.hagenmeyer@kit.edu

ABSTRACT

To bridge the temporal granularity gap in energy network design and operation based on Energy System Models, resampling of time series is required. While conventional upsampling methods are computationally efficient, they often result in significant information loss or increased noise. Advanced models such as time series generation models, Super-Resolution models and imputation models show potential, but also face fundamental challenges. The goal of time series generative models is to learn the distribution of the original data to generate high-resolution series with similar statistical characteristics. This is not entirely consistent with the definition of upsampling. Time series Super-Resolution models or imputation models can degrade the accuracy of upsampling because the input low-resolution time series are sparse and may have insufficient context. Moreover, such models usually rely on supervised learning paradigms. This presents a fundamental application paradox: their training requires the high-resolution time series that is intrinsically absent in upsampling application scenarios. To address the mentioned upsampling issue, this paper introduces a new method utilizing Generative Adversarial Transformers (GATs), which can be trained without access to any ground-truth high-resolution data. Compared with conventional interpolation methods, the introduced method can reduce the root mean square error (RMSE) of upsampling tasks by 10%, and the accuracy of a model predictive control (MPC) application scenario is improved by 13%. The implementation code for the model used in this paper has been publicly available at `https://github.com/KIT-IAI/ResampleGAN`.

Keywords Transformer, Generative Adversarial Network, Granularity Gap, Super Resolution, Smart Energy

1 Introduction

In recent years, the question of how energy systems can be decarbonized has received increasing attention due to global climate change and rising carbon dioxide emissions [1]. Energy System Models (ESMs) analyze energy system decarbonization pathways through mathematical modeling and simulation. Due to the complexity of these systems, multiple models often need to be coupled for joint analysis [2]. However, these independent models must compress the representation of temporal, spatial, or technological information for computational complexity reasons, leading to a loss of precision known as the granularity gap [3]. One direct consequence of this gap is that different models participating in joint simulations often run at their own inherent time resolutions. For instance, combining an electrical grid model (with a 15-minute resolution) with a gas network model (with an hourly resolution) creates temporal mismatches. Poncelet et al. [4] noted that choosing time series with different temporal resolutions can affect the simulation results. Therefore, accurately interpolating time-series data is essential for robust model coupling.

Researchers typically use conventional methods such as linear interpolation. These methods are simple and computationally efficient, but often fail to capture the complex nonlinear features inherent in data and tend to introduce noise. Advanced machine learning models offer viable alternatives but face fundamental limitations in this context. Time series generation models typically aim to synthesize new data for augmentation rather than faithfully upsampling specific

historical sequences. Meanwhile, state-of-the-art imputation methods like CSDI [5] and traditional Super-Resolution (Super-Resolution (SR)) models operate under a supervised or self-supervised masked training paradigm. This presents a critical application paradox: their training relies on the existence of ground-truth high-resolution data to calculate reconstruction loss (e.g., Root Mean Squared Error (RMSE)). However, in the target application scenarios of energy system coupling, such high-resolution data is intrinsically absent—if it existed, upsampling would not be necessary. Applying these models requires downsampling high-resolution data for training, which is impossible when only low-resolution data is available. Furthermore, when the input time series is sparse, models lacking global context mechanisms often suffer significant performance decline [6].

We formally examine the issue of time series super-resolution. Let $\mathcal{X}_{low} = \{x_L \in \mathbb{R}^{T_L}\}$ represent a collection of available low-resolution time series (e.g., hourly data), and let $\mathcal{X}_{high}$ denote the domain of a high-resolution time series (e.g., 15-minute data) with length $T_H > T_L$. Our goal is to learn a mapping function $G : \mathcal{X}_{low} \to \mathcal{X}_{high}$ such that the generated sequence $\hat{x}_H = G(x_L)$ maintains the temporal coherence of x_L while reconstructing the authentic high-frequency dynamics. The primary constraint is that we cannot acquire any authentic pairs (x_L, x_H) during the training process. The model must learn solely from $\mathcal{X}_{low}$ without direct supervision from $\mathcal{X}_{high}$, which means self-supervised.

To address this critical research gap, the present paper proposes a novel self-supervised time series super-resolution method that combines Transformer (TF) and Generative Adversarial Network (GAN). We utilize a TF backbone to capture global dependencies and discontinuities, enhanced with convolutional modules to explicitly maintain high-frequency local trends. To avoid the necessity for ground-truth high-resolution data, we utilize a GAN structure. This enables the substitution of conventional supervised loss functions, which necessitate unattainable high-resolution targets, with a feature-space constraint, allowing the model to acquire successful upsampling methods solely from low-resolution inputs.

The main contributions of the present paper include:

- **Novel Method**: We propose a novel self-supervised time series interpolation training framework that operates without the need for high-resolution ground truth. Unlike existing supervised SR or imputation methods, our method resolves the data paradox by learning exclusively from low-resolution inputs.
- **Real Application**: We demonstrate the structure preserving properties of our method in model predictive control (MPC) applications, highlighting its potential for real-world energy systems.

The subsequent sections of this paper are organized as follows. Section 3 outlines our methods. Section 2 presents a review of related work. Section 4 describes the experimental setup and data analysis and Section 5 concludes a conclusion and an outlook.

2 Related Work

Data intertransformation is an unavoidable problem in the interaction between different models during the co-simulation. As mentioned in Sec. 1, efficiently and accurately transforming time-series data is essential for achieving accurate model coupling and minimizing errors caused by temporal mismatches. To address the temporal mismatch issue, researchers frequently employ resampling techniques. These include upsampling for filling in low-resolution data [7] and downsampling for condensing high-resolution data [8]. Compared with downsampling, upsampling of data is more prone to introducing errors. Upsampling necessitates the creation of new data points via interpolation or alternative estimation techniques. Interpolation is a widely used time series resolution upsampling method, but its applicability is limited to the specific characteristics of the dataset [9]. For instance, Omoyele et al. [10] evaluated time series upsampling methods in energy systems. Their study focused on two key data categories: solar and wind. For solar data, the non-dimensional technique offers better results. For wind data, a mix of physical models and stochastic fluctuations is more successful.

Lepot et al. [7] reviewed a variety of interpolation methods and pointed out that most interpolation methods lack an evaluation framework separate from specific algorithms, making it difficult to establish universal performance benchmarks. Additionally, each upsampling method is based on specific assumptions about the data's characteristics. When the data does not align with these assumptions, the quality of the generated data is significantly compromised.

To address the limitations of traditional upsampling methods, researchers have increasingly turned to advanced machine learning techniques, such as time series generation, SR and imputation models. Traditional time series generation models focus on learning and reconstructing the underlying distributions of original data to generate new high-resolution sequences with similar statistical properties. The concept of SR originates from computer vision, aiming to establish an

accurate mapping from a low-resolution sequence to a high-resolution sequence. Time series imputation is a broader concept that refers to various techniques for filling in missing data points.

Super-Resolution (SR) is a crucial technique for enhancing data resolution. SR combines upsampling with deep neural networks to recover more details by learning from low- and high-resolution data. SR not only increases the sampling rate of the time series, but also uses methods such as deep learning to recover or reconstruct the lost details and high-frequency information in the time series. It is making the result closer to the real high-sampling time series. It is widely used in image processing [11], point cloud reconstruction [12], and other fields. However, compared to the popularity of SR in the field of images and point clouds, there are relatively few studies on SR in the field of time series. Han and Wang [13] are the first researchers to apply the combination of Recurrent Neural Network (RNN) and GAN to generate high-resolution temporal volume sequences. However, the training process requires the use of real high-resolution data to calculate the loss. In practical situations, this presents a paradox: if the high-resolution data already exists, why is there a necessity to interpolate it from low-resolution data?

This data availability challenge also exists in the field of time series imputation, which shares similar methodological foundations with the upsampling task. Time series imputation focuses on filling missing values in a series, which can also be considered a special case of upsampling. Important research in this area includes GRU-D [14], which modifies the Gated Recurrent Unit (GRU) to incorporate missing pattern information, BRITS [15], which leverages bidirectional recurrent dynamic systems to learn imputation, and CSDI [5], which learns to reverse a diffusion process to reconstruct missing data points. These models are typically trained in a self-supervised paradigm, where values are artificially masked from the full real dataset and the model's task is to reconstruct these masked values accurately. Thus, similar to the challenges in time series SR, the training process of these imputation models also presupposes the availability of complete data, which contradicts the unavailability of high-resolution data in upsampling tasks. Moreover, in upsampling tasks, known points are typically sparse, resulting in the model having limited reference data points during input, which can easily lead to insufficient contextual information and suboptimal outcomes [6].

Although the goals of traditional generative models and upsampling tasks are inconsistent, advanced generative models (such as generative adversarial networks (GANs) or diffusion models) can achieve upsampling through "conditional generation" [16]. GANs are artificial intelligence methods used to solve the sample generation problem [17]. Its goal is to study a set of training samples, learn the probability distribution that generates those samples, and generate additional samples based on this probability distribution. Tang et al. [18] interpolated solar data using GANs, marking the first use to generate time series with different resolutions [10]. Moreover, its limitation is that the model structure is bound to a specific resolution and length. The model structure is hardcoded for specific use cases. It works only with two fixed temporal resolutions and lengths, such as a 30-minute input and a 5-minute output resolution. However, most research [19, 20] on time series GAN focuses on data enhancement, i.e., techniques aimed at improving the quality of existing datasets through synthetic data generation. The MC-TimeGAN introduced by Demirel et al. [21] can generate multivariate synthetic time series conditioned on labels, focusing on synthetic grid congestion scenarios. Their work mentioned the possibility of generating time series with varying resolutions. However, the core goal of their research is to generate event-specific conditional data, not a generalized resolution conversion tool. Therefore, although GANs have great potential in ensuring high fidelity of generated data, existing work has not yet provided a mature framework that can adapt to arbitrary resolutions and is designed explicitly for unsupervised upsampling tasks.

In addition to the pursuit of high fidelity, it is also crucial to address the issue of insufficient contextual information caused by sparse input points. In this regard, the Transformer (TF) architecture demonstrates significant advantages thanks to its attention mechanism. This mechanism captures long-term time dependencies and complex multivariate correlations while enabling parallel processing [22]. These properties have been successful in several areas, including time series prediction, classification, and anomaly detection [23]. However, relatively little work has focused on time series upsampling. Multi-scale attention [24] and frequency-domain attention [25] represent significant advancements in the TF architecture. The multi-scale attention mechanism offers significant advantages for resolution transformation. It enables the model to simultaneously capture local patterns and global trends at different temporal granularities. This capability is critical for maintaining or reconstructing information while transforming resolution [24]. The frequency-domain attention mechanism provides another advantage. It enables TFs to directly manipulate spectral components, offering a more principled method to resolution conversion. This method maintains significant frequency features [25]. The application of these mechanisms demonstrates the potential of TFs in resampling tasks, as they can adaptively focus on the most relevant temporal and spectral features to achieve accurate resolution conversion.

TFs focus on understanding dependencies between data points, while GANs demonstrate superior skill in creating high-quality synthetic data. Together, they provide a reasonable method for time series upsampling. In the coupling of energy network models, the input and output time series resolution is often not fixed, thereby the GANs structure has to be designed to be adaptive to different resolutions. Through the above analysis, existing research has shortcomings in the following aspects:

- **Context**: When the input data points are extremely sparse, the model lacks sufficient context for the task.
- **Fidelity**: Traditional upsampling methods may lose details and local features in the original data.
- **Data Dependency**: The requirement of the upsampling task itself is based on the fact that high-resolution data is missing. However, there is no method for training entirely based on low-resolution data.

3 Methodology

To address the limitations identified in Section 2, this paper presents an adaptive convolutional TF-GAN hybrid architecture for time series SR. The training process is mainly divided into three stages:

- **Stage 1** is mainly used for pre-training the generator.
- **Stage 2** is mainly used for pre-training the feature space discriminator.
- **Stage 3** is mainly used for joint-training of the generator and discriminator.

The main design attributes will be introduced in the following subsections individually and the design decisions address three specific challenges:

1. **Why choose TF?** Energy profiles frequently exhibit discontinuities and sudden transitions, including as unexpected demand fluctuations or solar ramp events. Our analysis in the baseline comparison (refer to Appendix A) illustrates that TF substantially surpass LSTM and TCN models in the reconstruction of non-smooth waveforms. The TF's attention mechanism captures the global dependencies essential for maintaining structural integrity over sparse inputs. This can reduce the impact of insufficient context.
2. **Why Utilize Convolution?** While effective at modeling global context, pure self-attention mechanisms can sometimes smooth out high-frequency details. However, Energy data contains critical local peaks and short-term trends. A convolutional multi-head attention module can explicitly extract and model these local trends.
3. **What is the rationale behind using GAN?** The choice to employ a GAN is driven by the fundamental challenge of defining a valid loss function between sequences of differing lengths. In our upsampling/SR task, the input low-resolution sequence x_{low} and the output high-resolution sequence x_{high} represent the same temporal period but possess different vector lengths ($T_{low} \neq T_{high}$). This length mismatch renders traditional point-wise error metrics (e.g. RMSE) semantically incorrect or infeasible to compute directly without artificial interpolation. To address this, we implement a feature space loss that quantifies the similarity between the two sequences in a high-dimensional latent feature space instead of the temporal domain. However, this method necessitates a feature extractor capable of encoding complex temporal dynamics. The Discriminator in the GAN framework serves precisely this purpose: through adversarial training, it learns to extract robust feature representations of energy data, acting as a dynamic feature extractor that allows the Generator to learn structural consistency from multi-resolution data.

3.1 Generator

A critical step in building a generative model for time series SR is selecting a suitable core generator architecture. Real-world data often exhibits significant variability. It may show different sample resolutions, contain missing values, and display periodic or seasonal trends. An effective model requires adaptability to deal with these features. Therefore, in the present paper, TF is used as the base model for the generator with its powerful sequence modeling capabilities and flexible architecture design. For details on the reasons for choosing TF as the base model, see Appendix A.

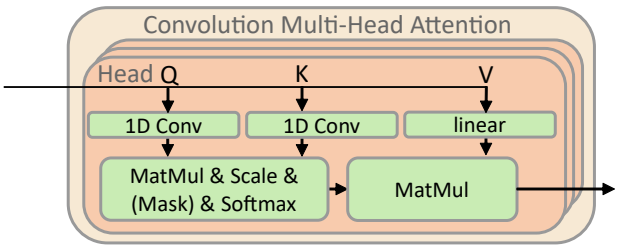

Figure 1: Modified attention mechanism used in the convolutional multi-head attention module.

Transformers utilize a self-attention mechanism that enables a model to process sequence elements in parallel and learn global dependencies [22]. The mechanism generates three vectors based on the input sequence: query (**Q**), key (**K**), and value (**V**) matrices, where queries and keys determine attention weights while values carry the actual information to be aggregated. **Q** and **K** must have the same dimension, but **v** can have a different dimension, allowing it to map the input information into an output of a different dimension (or "length"), which is exactly what is needed for time series SR tasks (generating a high-resolution sequence from a low-resolution one). In the present paper, the task is to change the temporal resolution. Data points must be added, removed, or converted from the original dataset. Therefore, the short-term trend of the data points is of interest. Increasing the trend attention helps the data points recognize short-term patterns and better insert new points or delete old points. To address this need, a convolutional multi-head attention module [26] is employed, as illustrated at the top of Fig. 1. This module explicitly models trend changes in the data by capturing local contextual information for each data point. It ensures that each data point is aware of its context. The module uses 1D convolutional layers to extract these local trends, enhancing the model's understanding of short-term patterns.

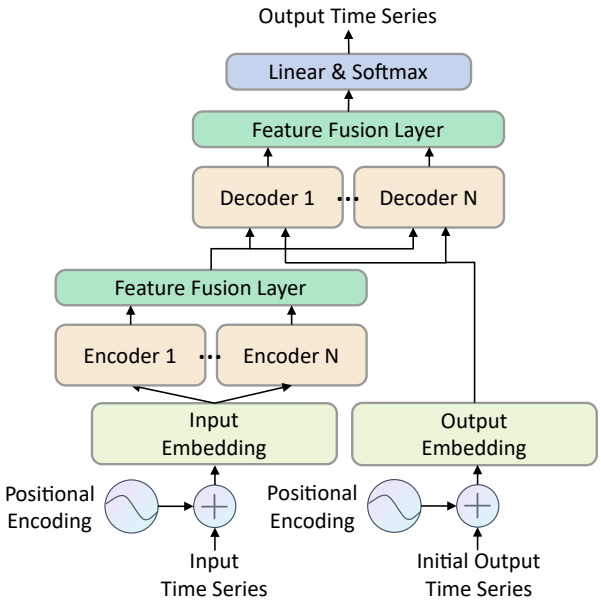

Figure 2: Generator of the modified GAN, consisting of encoder–decoder layers with feature fusion.

The outputs of the two attention mechanisms are combined in a feature fusion layer, resulting in a final feature matrix. A detailed description of this feature fusion layer (Multi-Scale Attention Aggregation [27]) can be found in Appendix B.

It is essential to note that due to the task of SR involved in the present work, all data point transformations are performed in the known time domain. Therefore, the causal masked multi-head attention mechanism will not be used.

In summary, the generator G used in the present paper is demonstrated in Fig. 2. It receives the following input:

- Input time series $X_{\text{input}} \in \mathbb{R}^{T_{\text{input}}}$ with the length of input time series T_{input}.
- Initial output time series $X_{\text{init}} \in \mathbb{R}^{T_{\text{output}}}$ with the length of output time series T_{output}. The initial time series is obtained by linear interpolation.

X_{input} is first embedded and then passed through the convolution encoder and the Fast Fourier Transform (FFT) encoder. After processing, the corresponding feature matrices are obtained. These feature matrices are fed into a feature fusion layer to produce the encoder's output. The encoder's output, along with X_{init}, is then provided to the decoder to generate the final output time series X_{output}. Using the above Transformer structure, it is possible to realize a generator G that supports input and output at arbitrary temporal resolution.

3.2 Discriminator

Although the combined loss function can improve the fit in terms of statistical features, it does not improve the fit when training the generator without the actual target data. However, such loss functions typically promote conservative

forecasts and eventually converge to the mean. Furthermore, it is both impractical and futile to exhaust all the indicators. Simultaneously, conflicts may arise among several indicators, resulting in unreasonable training. By introducing the discriminator in the GAN, the model is able to learn implicit features of data. These features are difficult to encode through deterministic indicators [19, 28, 29]. The discriminator attempts to distinguish between authentic data from reality and synthetic data produced by the generator by learning the characteristics and distribution of the real data. In an ideal adversarial training process, the generator and the discriminator are trained together. Ultimately, the generator is capable of producing data that is indistinguishable from real data.

However, when dealing with tasks involving data of different lengths, such as resampling, a simple discriminator can easily distinguish between real data and generated data by only learning superficial representations such as sequence length, instead of learning the complex dynamic patterns within the sequence. Thus, the generator is not able to receive meaningful feedback, which hinders its learning ability. Furthermore, a standard mode collapse [30] problem arises in GAN training. That is, the structure of the discriminator may be too robust, causing its loss to converge to zero quickly. This results in the generator failing to receive an effective gradient signal, causing the training process to stagnate completely.

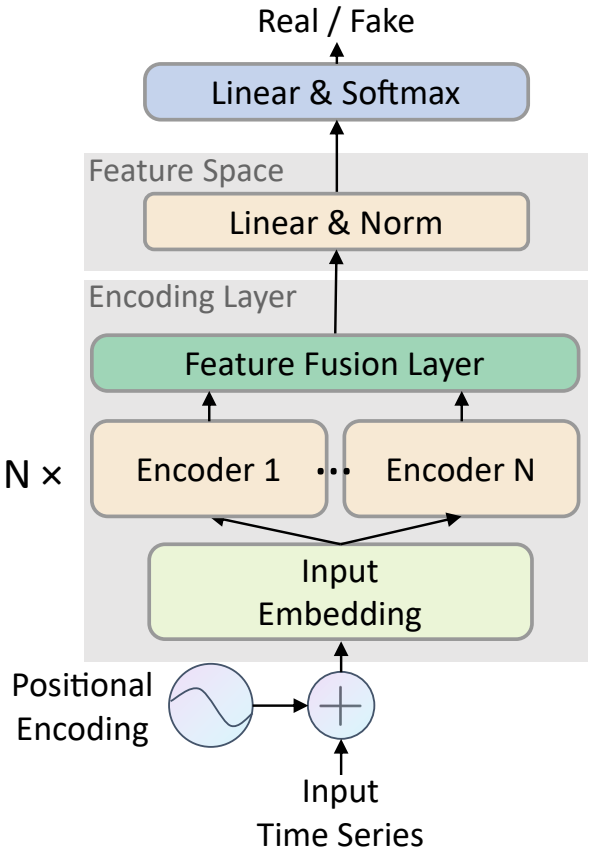

Figure 3: Discriminator of the modified GAN, consisting of Feature Space layers.

To address both challenges simultaneously, real and synthetic data will be distinguished in feature space, and a feature matching mechanism [30] will be introduced, as shown in Fig. 3. The core idea of this method is to adjust the optimization goal of the generator, which is no longer to maximize the classification error rate of the discriminator, but to make the features extracted from the generated data in the middle layer of the discriminator as similar as possible to the features of the real data. Specifically, the difference between the output of real and generated data in the discriminator's feature extraction layer is used as a new loss term to train the generator. Even if the discriminator has become very powerful and can perfectly distinguish between real and fake data, the generator can continue to learn and optimize by minimizing the feature differences between real and generated data. At the same time, the feature matching mechanism requires the generator to make the features of the generated data in the middle layer of the discriminator

consistent with the real samples, thereby indirectly guiding the discriminator to focus on deeper feature expressions rather than simple surface features.

3.3 Loss Function

As our goal is neither predictive (autoregressive) nor sequence classification, conventional error measures as objectives such as RMSE or Mean Absolute Error (MAE) are unsuitable for the generator. This is especially true in our multi-resolution context, where the input x_{input} and the produced output $\hat{x}$ vary in both length and temporal granularity. The differences preclude direct point-wise comparison and require a loss design that is resilient to temporal misalignment and semantic variance. To address these issues, a combined loss function is implemented. It combines various loss functions to direct training. The primary design objective is to maintain both local numerical precision and global structural integrity while ensuring adaptability across various input resolutions. The total loss is a weighted sum of all loss functions:

$$\mathcal{L}_{\text{total}} = \sum_i \lambda_i \mathcal{L}_i \tag{1}$$

Learnable weights [31] λ_i via a softPlus transformation are implemented to ensure the stability of the training process:

$$\lambda_i = \log\left(1 + e^{\alpha_i}\right), \quad \alpha_i \in \mathbb{R} \tag{2}$$

where α_i is the learnable parameter updated by backpropagation and the optimizer. These weights are trained jointly with the generator, enabling the model to emphasize the most informative supervision signals during learning dynamically. All initial weights are 1.

The following loss functions are employed in the training model stages of the present paper. The sliding window is employed to handle extended sequences when computing the indicators, which necessitates sequences of uniform length.

- Mean Squared Error

$$\mathcal{L}_{\text{mse}} = \text{MSE}\left(\text{Window}(X_{\text{output}}), X_{\text{input}}\right) \tag{3}$$

- Smoothness Loss

$$\mathcal{L}_{\text{smoothness}} = \text{Mean}\left(\left(\Delta^2(X_{\text{output}})\right)^2\right) \tag{4}$$

$$\Delta^2(X) = (x_{t+2} - x_{t+1}) - (x_{t+1} - x_t) \tag{5}$$

- Gradient Loss

$$\mathcal{L}_{\text{gradient}} = \text{MSE}\left(\Delta\text{Window}(X_{\text{output}}), \Delta X_{\text{input}}\right) \tag{6}$$

$$\Delta(X) = (x_{t+1} - x_t) \tag{7}$$

- Feature Matching Loss

$$\begin{aligned}\mathcal{L}_{\text{FM}} = &||\mu(F_{X_{\text{input}}}) - \mu(F_{X_{\text{output}}})||_2^2 \\ &+ ||\sigma(F_{X_{\text{input}}}) - \sigma(F_{X_{\text{output}}})||_2^2\end{aligned} \tag{8}$$

First, Mean Squared Error (MSE) Loss is used to maintain the global low-resolution fidelity of the sequence. It ensures that the generated curve is strictly anchored to the original low-resolution input in terms of macroscopic trends, preventing numerical drift in the generated data. Second, Gradient Loss is introduced to address the high-resoltion transient features common in energy data. Using MSE alone often leads to over-smoothing of the generated results. Gradient Loss forces the model to focus on local rates of change, thus accurately preserving key waveform information. Third, Smoothness Loss acts as a regularization term. By limiting the second-order difference, it suppresses noise that may be caused by abrupt changes in the second-order difference during upsampling. Finally, to address the core challenge of self-supervised learning in this study—the lack of high-resolution ground truth during the training phase—we introduce Feature Matching Loss. Unlike the point-based loss mentioned above, this term uses the high-dimensional feature distribution extracted by the discriminator to guide the generator, ensuring that the generated data approximates the real data distribution in terms of statistical properties and implicit patterns.

3.4 Training Architecture

The whole training process is mainly divided into three stages, including pre- and joint-training processes. In the first stage, the generator focuses on pre-training. The generator is responsible for capturing the complex patterns and long-distance temporal dependencies of the time series. It receives the input data X_{input} and pre-processed initial X_{initial}, and is trained using the combined loss $\mathcal{L}_{\text{total}}$ to generate a high-resolution output time series.

The second stage aims to jointly train the feature space discriminator to obtain a usable feature space for the third stage. In this stage, the discriminator is jointly trained on the input data X_{input} and the output data X_{output} to learn how to distinguish between them effectively. At the same time, the generator is also trained with $\mathcal{L}_{\text{total}}$ and $\mathcal{L}_{\text{FM}}$ to ensure that the output data X_{output} matches the input data X_{input} in the feature space. The loss function of the discriminator in this stage uses Binary Cross-Entropy Loss (BCELoss) [32].

$$\begin{aligned}\mathcal{L}_{\text{D}} = & -\mathbb{E}_{X_{\text{input}}\sim p_{\text{data}}}\left[\log D(X_{\text{input}})\right] \\ & -\mathbb{E}_{X_{\text{output}}\sim p_g}\left[\log(1-D(X_{\text{output}}))\right]\end{aligned} \tag{9}$$

In the third stage, the trained discriminator is used as a feature space extractor. The generator continues to be trained separately using the extracted high-dimensional features. The core goal of the third stage is to learn how to generate time series data that is sufficient to deceive the discriminator. The output data X_{output} will match closely with the input data X_{input} in the feature space, ultimately achieving better time series upsampling.

4 Results

This section presents the experimental results of the present paper. First, the data set used will be introduced, followed by a performance evaluation of the model and an analysis of the results. Then, an application scenario is introduced. All single training results in the present paper were completed on a computer equipped with a 4070ti super GPU and a 7800x3d CPU.

4.1 Dataset

The WPuQ [33] dataset records the electric load data of 38 households in a small village in Lower Saxony, Germany. To ensure the quality of the training data and computing power limitations, we selected 6 indices that have the longest continuous non-interrupted record. The present paper utilizes the power data P1 from 2018.

PV-Live [34] is Europe's leading minute-level solar irradiance dataset, providing high-resolution measurements over the state of Baden-Württemberg, Germany. The dataset has been maintained collaboratively since September 2020, encompassing data from 40 measurement stations with a one-minute resolution. Similarly, we selected 6 stations based on the same criterion. The present paper utilizes their 363-day Solar Radiation (Gg_pyr) data in 2023 for the experiment.

The Wind Power dataset [35] contains data from 1 second to every hour, compared to the typical 10-minute interval for European wind power data. The present paper utilizes the entire dataset (81 days) for the experiment.

The mini-photovoltaic (MPV) benchmark dataset, known as MPVBench [36] contains real-time measurement data from five MPV, also known as balcony power plants in the Karlsruhe and Pforzheim regions. The present paper utilizes the entire 364-day solar power data from all locations.

All data are resampled to 15-minute and 5-minute intervals, spanning 1 day, to verify the model's performance at varying intervals.

4.2 Ablation Experiment

First, an ablation experiment is conducted on the training architecture and attention mechanism structure introduced in this paper. The results for this experiment are derived from an average of 10 independent model training samples. Tab. 1 summarizes the performance at different training stages (Stages) and different methods (Methods) for different datasets (WPuQ [33], PV-Live [34], Wind Power [35], MPVBench [36]). Italic and underlined numbers indicate the best performance within a single stage, while bold numbers indicate the best performance across all stages. The evaluation indicators include the root mean square error (RMSE) and the Pearson Correlation Coefficient (PCC). The results for each dataset are presented separately for the training set (Train) and the test set (Test). Additionally, Static refers to the linear interpolation, Gauss Process, Cubic interpolation and DL (Deep Learning) refers to CSDI [5], BRITS [15], SRGAN [37] are used as performance benchmarks. In order to adapt to the time series upsampling task, the mask used

Table 1: Performance Comparison - RMSE and PCC Metrics (lower RMSE and higher PCC indicate better performance) on the WPuQ [33], PV-Live [34], Wind Power [35], MPVBench [36] data sets for upsampling from 15-min to 5-min

Metric	Stage	Method	WPuQ [W]		PV-Live [W/m^2]		Wind Power [W]		MPVBench [W]	
			Train	Test	Train	Test	Train	Test	Train	Test
PCC	Stage 1	CONV	0.8996	0.8940	0.9256	0.9243	0.9477	0.9367	0.9384	0.9356
		SELF	0.8150	0.7971	0.8034	0.8030	0.8455	0.8270	0.7886	0.7864
		S+C	*0.8997*	*0.8942*	*0.9352*	*0.9327*	0.9534	0.9426	*0.9437*	*0.9411*
		S_C	0.8967	0.8896	0.9237	0.9221	*0.9597*	*0.9506*	0.9329	0.9297
	Stage 2	CONV	0.9288	0.9141	0.9824	0.9816	0.9699	0.9600	0.9845	0.9829
		SELF	0.8263	0.8099	0.8058	0.8072	0.8552	0.8409	0.8029	0.8007
		S+C	0.9274	*0.9143*	0.9824	0.9817	0.9701	0.9597	0.9844	0.9829
		S_C	*0.9313*	0.9141	*0.9825*	*0.9817*	*0.9706*	*0.9602*	*0.9848*	*0.9829*
	Stage 3	CONV	0.9384	0.9118	0.9836	0.9813	0.9713	0.9596	0.9861	0.9825
		SELF	0.8264	0.8085	0.8049	0.8064	0.8476	0.8328	0.8008	0.7981
		S+C	0.9357	**0.9122**	0.9838	0.9813	0.9716	0.9596	0.9861	*0.9825*
		S_C	**0.9421**	0.9108	**0.9843**	*0.9813*	**0.9727**	*0.9598*	**0.9871**	0.9822
	Static	Cubic	0.9091	0.9041	0.9795	0.9791	0.9645	0.9551	0.9827	0.9817
		GP	0.9166	0.9093	*0.9819*	**0.9815**	*0.9693*	**0.9604**	*0.9842*	**0.9833**
		Linear	*0.9166*	*0.9119*	0.9819	0.9814	0.9689	0.9600	0.9841	0.9833
	DL	CSDI	0.6456	0.6173	0.9482	0.9466	0.8271	0.7649	0.9291	0.9257
		BRITS	0.5266	0.5108	0.9557	0.9544	0.9373	0.9204	0.9350	0.9348
		SRGAN	*0.8844*	*0.8633*	*0.9742*	*0.9721*	*0.9571*	*0.9413*	*0.9773*	*0.9747*
RMSE	Stage 1	CONV	*0.1829*	*0.1845*	0.2187	0.2178	0.1934	0.2050	0.1541	0.1593
		SELF	0.2646	0.2697	0.3434	0.3392	0.3352	0.3378	0.2870	0.2921
		S+C	0.1840	0.1852	*0.2042*	*0.2053*	0.1851	0.1972	*0.1483*	*0.1532*
		S_C	0.1877	0.1898	0.2214	0.2208	*0.1753*	*0.1856*	0.1599	0.1649
	Stage 2	CONV	0.1502	0.1608	0.1072	0.1081	0.1521	0.1678	0.0818	0.0868
		SELF	0.2538	0.2588	0.3399	0.3344	0.3227	0.3232	0.2769	0.2819
		S+C	0.1516	0.1610	0.1072	0.1081	0.1517	0.1684	0.0820	0.0869
		S_C	*0.1469*	*0.1599*	*0.1068*	*0.1079*	*0.1504*	*0.1673*	*0.0808*	*0.0868*
	Stage 3	CONV	0.1400	0.1618	0.1034	0.1090	0.1483	0.1684	0.0773	0.0879
		SELF	0.2536	0.2595	0.3401	0.3345	0.3306	0.3310	0.2778	0.2831
		S+C	0.1420	0.1625	0.1029	0.1092	0.1477	0.1685	0.0775	*0.0878*
		S_C	**0.1360**	*0.1625*	**0.1013**	*0.1091*	**0.1452**	*0.1684*	**0.0744**	0.0885
	Static	Cubic	0.1699	0.1711	0.1155	0.1153	0.1656	0.1780	0.0861	0.0896
		GP	*0.1590*	0.1619	*0.1084*	**0.1083**	*0.1533*	**0.1666**	*0.0822*	**0.0854**
		Linear	0.1604	**0.1618**	0.1085	0.1084	0.1543	0.1676	0.0823	0.0855
	DL	CSDI	0.3565	0.3639	0.1839	0.1840	0.3639	0.4066	0.1734	0.1803
		BRITS	0.3782	0.3733	0.2286	0.2273	0.3289	0.3319	0.2540	0.2568
		SRGAN	*0.1869*	*0.1982*	*0.1293*	*0.1326*	*0.1806*	*0.2028*	*0.0984*	*0.1052*

by the imputation model will be fixed. That is, a high-resolution signal is recovered from a fixed, sparse low-resolution signal.

The attention mechanisms used in our method include:

- SELF, which refers to the traditional Transformer self-attention mechanism,
- CONV, the convolutional attention mechanism used in this paper,
- S+C, the serial combination of the self-attention layer and the convolutional attention layer, and
- S_C, the parallel connection of the self-attention mechanism and the convolutional attention mechanism through the feature fusion layer.

The best model in each stage is saved independently based on the loss performance of the test set during training. The training of the subsequent stage is based on the best model of the previous stage, but the best test set loss from the previous model will not be recorded. The values shown in Tab. 1 are the comparison between the output data X_{output} and the real data X_{real}. It should be emphasized that the real data X_{real} has never been used in training. Only the input data X_{input} is used to calculate the training loss during the entire training process.

The performance of current benchmark models is first evaluated. In Tab. 1, stage Static and DL show that the RMSE is significantly lower for both Gaussian processes and linear interpolation than for the DL method. There is only a little difference in performance between the Gaussian process and linear interpolation, while the SRGAN model for

image super-resolution is the best performing among all deep learning models, it still cannot outperform simple linear interpolation models. SRGAN's ability to recover high-frequency details often manifests as additional noise in this scenario, thus reducing the effectiveness of super-resolution. For interpolation models, in time series upsampling tasks, the target high-resolution sequence is often several times longer than the low-resolution sequence. This leads to a very sparse mask matrix of known points and can dramatically increase the uncertainty of the imputation model, ultimately leading to suboptimal upsampling results.

After analyzing the performance of existing baseline models, the contributions of the introduced method and its key components will now be evaluated. From Tab. 1, Stage 2 and Stage 3 generally have a better model performance than Stage 1 on all datasets, performance indicators (RMSE, PCC), and training and test sets. This result clearly indicates that introducing the discriminator structure can significantly improve the model's training quality. Taking the RMSE on the test set of the WPuQ dataset as an example, the RMSE of S+C in Stage 1 is 0.1840, while the RMSE of S+C in Stage 2 is reduced to 0.1516, a decrease of about $21.37\ \%$. For the PV-Live test set, the RMSE of CONV in Stage 1 is 0.2187, while the RMSE in Stage 2 is reduced to 0.1072, a decrease of about $50.98\ \%$. In contrast, the model using only the SELF method yielded relatively poor results in all indicators across all training stages and nearly all datasets. This indicates that for such SR tasks, the self-attention mechanism alone is insufficient to capture and utilize the key information in the data effectively. This proves that the introduction of convolutional attention is practical. For example, on the wind test set, the RMSE of SELF in Stage 1 is 0.3378, while S+C is 0.1972, and SELF is about $41.62\ \%$ higher.

The S_C method usually achieves lower RMSE and higher PCC, indicating that the parallel structure is more suitable for accurately fitting the training data. The bold numbers in the table show that the S_C structure of Stage 3 achieves the best results on almost all training sets. Compared with the static interpolation method used as a benchmark, the S_C structure has an average performance lead of $10.48\ \%$ in RMSE. In PCC, this value is $0.9\ \%$. In contrast, the model's generalization ability is relatively average. Compared to linear interpolation, the RMSE increases by approximately $0.5\ \%$. This phenomenon demonstrates the significant difference between our proposed method and traditional prediction models in terms of application paradigm. Unlike time series forecasting, which requires inferring unknown futures, SR tasks in practical applications always involve complete low-resolution input data. Since our proposed method employs a fully self-supervised learning paradigm, and the training process does not rely on any external high-resolution ground truth, this high fit on the training set should not be considered harmful overfitting, but rather transductive learning. The model's performance on the training set proves that it can utilize the attention mechanism of the transformer and the adversarial constraints of GANs to obtain the statistical distribution and structural features of the target data. This indicates that in practical tasks, targeted training (or fine-tuning) for each target dataset is a superior strategy, providing more faithful reconstruction results than generalized models without concern for limitations in generalization ability.

To verify the validity of the above conclusions, a significance test was performed. Tab. 2 and Tab. 3 are tables about statistical significance tests and performance differences. These tests ensure that the observed performance differences are not accidental, but consistent. In the Tab. 2 and Tab. 3, the p-values more than 0.05 (i.e., statistically not significant) are marked in bold. For RMSE, when Diff is negative, the performance improves. For PCC, when Diff is positive, the performance improves.

Table 2: Stage Comparison - Statistical Significance Tests and Performance Differences

		WPuQ				**PV-Live**				**Wind Power**				**MPVBench**			
		train		test		train		test		train		test		train		test	
		pval	diff	pval	diff	pval	diff	pval	diff	pval	diff	pval	diff	pval	diff	pval	diff
PCC	stage 2 vs. 1	0.000	0.035	0.000	0.025	0.000	0.059	0.000	0.060	0.001	0.011	0.016	0.010	0.000	0.052	0.000	0.053
	stage 3 vs. 2	0.000	0.011	0.000	-0.003	0.000	0.002	0.000	0.000	0.000	0.002	**0.281**	0.000	0.000	0.002	0.000	-0.001
RMSE	stage 2 vs. 1	0.000	-0.041	0.000	-0.030	0.000	-0.115	0.000	-0.113	0.001	-0.025	0.008	-0.018	0.000	-0.079	0.000	-0.078
	stage 3 vs. 2	0.000	-0.011	0.000	0.003	0.000	-0.006	0.000	0.001	0.000	-0.005	**0.373**	0.001	0.000	-0.006	0.000	0.002

From Tab. 2, whether it is RMSE or Pearson Correlation Coefficient (PCC) for four datasets (WPuQ, PV-Live, Wind, MPVBench), Stage 2 show statistically significant performance improvements compared to Stage 1. This can be clearly observed from the "Stage 2 vs. 1" rows: The vast majority of p-values are far below the 0.05 significance level, which indicates that these stage improvements are systematic effects. At the same time, these low p-values are accompanied by significant performance differences, e.g., the Diff of Stage 2 vs 1 in the PCC part is generally 0.01 to 0.059. This broad and consistent improvement highlights the significant enhancement of model generalization ability and prediction accuracy brought about by the introduction of the discriminator. Regarding the comparison between Stage 2 and Stage 3, although the differences between the two stages are mostly statistically significant in terms of p-values, Stage 3 exhibits only a slight numerical advantage in most cases. This indicates that although stage 3 is an improvement over stage 2, it is not as significant as stage 2's improvement over stage 1.

After determining Stage 3 as the optimal training paradigm, we further evaluated the effectiveness of different model architectures, as shown in Tab. 3. S_C significantly outperformed the pure self-attention architecture SELF on all

Table 3: Method Comparison - Statistical Significance Tests and Performance Differences

		electric				**pv**				**wind**				**mpv**			
		train		test		train		test		train		test		train		test	
		pval	diff	pval	diff	pval	diff	pval	diff	pval	diff	pval	diff	pval	diff	pval	diff
PCC	vs. CONV	0.003	0.004	**0.369**	-0.001	0.000	0.001	**0.790**	0.000	0.002	0.001	**0.918**	0.000	0.001	0.001	**0.094**	0.000
	vs. SELF	0.000	0.116	0.000	0.102	0.000	0.179	0.000	0.175	0.000	0.125	0.000	0.127	0.000	0.186	0.000	0.184
	vs. S+C	0.000	0.006	0.010	-0.001	0.000	0.000	**0.997**	0.000	0.037	0.001	**0.875**	0.000	0.001	0.001	0.013	0.000
RMSE	vs. Conv	0.003	-0.004	**0.694**	0.001	0.000	-0.002	**0.944**	0.000	0.033	-0.003	**1.000**	0.000	0.000	-0.003	**0.226**	0.001
	vs. SELF	0.000	-0.118	0.000	-0.097	0.000	-0.239	0.000	-0.225	0.000	-0.185	0.000	-0.163	0.000	-0.203	0.000	-0.195
	VS. S+C	0.000	-0.006	**1.000**	0.000	0.000	-0.002	**0.900**	0.000	**0.167**	-0.003	**1.000**	0.000	0.000	-0.003	**0.109**	0.001

datasets and across all evaluation metrics, indicating that a simple global attention mechanism cannot cope with the sparsity and local fluctuations of energy data. Secondly, compared to strong baseline models containing convolutional components (CONV and S+C), S_C exhibited superior feature fitting capability. On the training set, the performance improvement of S_C reached statistical significance on multiple complex datasets. For example, on the MPV dataset, compared to the serial structure S+C, S_C has a p-value of 0.001 on the PCC metric and achieves a significant reduction of 0.003 on the RMSE ($p = 0.000$); on the Electric dataset, the advantage of S_C over CONV is also significant (p-values for both PCC and RMSE are 0.003). The generalization performance differences among various fusion strategies on the test set lacked statistical significance ($p > 0.05$). However, the consistent advantage observed in the training set suggests that the attention fusion design can more efficiently leverage both global dependencies and local features concurrently, thereby improving the reconstruction accuracy of high-resolution time series.

Table 4: Performance Comparison - RMSE and PCC Metrics (lower RMSE and higher PCC indicate better performance) on the WPuQ [33], PV-Live [34], Wind Power [35], MPVBench [36] data sets for upsampling from 1-hour to 15-min

Metric	**Stage**	**Method**	**WPuQ** [W]		**PV-Live** [W/m^2]		**Wind Power** [W]		**MPVBench** [W]	
			Train	Test	Train	Test	Train	Test	Train	Test
PCC	Stage 3	CONV	0.8544	0.8094	0.9660	**0.9521**	0.9210	**0.9090**	0.9624	0.9500
		SELF	0.6649	0.6570	0.7355	0.7297	0.7792	0.7556	0.7195	0.7201
		S+C	0.8665	0.8195	0.9546	0.9362	0.8861	0.8542	0.9761	**0.9553**
		S_C	**0.8894**	**0.8208**	**0.9785**	0.9507	**0.9251**	0.9027	**0.9765**	0.9489
	Static	Cubic	0.7877	0.7864	0.9500	0.9467	0.9135	0.9012	0.9517	0.9552
		GP	0.7896	0.7865	0.9530	0.9496	0.9130	0.9043	0.9469	0.9501
		Linear	*0.8034*	*0.8018*	*0.9562*	*0.9533*	*0.9231*	*0.9151*	*0.9568*	*0.9596*
RMSE	Stage 3	CONV	0.2360	0.2675	0.1536	0.1775	0.2561	0.2660	0.1374	0.1608
		SELF	0.3876	0.3866	0.4056	0.3984	0.4027	0.4082	0.3575	0.3643
		S+C	0.2280	0.2644	0.1689	0.2023	0.3150	0.3508	**0.1086**	**0.1522**
		S_C	**0.2051**	**0.2628**	**0.1226**	**0.1802**	**0.2443**	**0.2702**	0.1097	0.1619
	Static	Cubic	0.2909	0.2905	0.1874	0.1884	0.2654	0.2759	0.1556	0.1526
		GP	0.2841	0.2829	0.1802	0.1815	0.2623	0.2663	0.1611	0.1592
		Linear	*0.2733*	*0.2727*	*0.1743*	*0.1751*	*0.2482*	*0.2529*	*0.1459*	*0.1438*

To further evaluate the model's robustness to sparser inputs, we conducted experiments ranging from 1 hour to 15 minutes (4x upsampling rate), the results of which are summarized in Table 4.1. Consistent with prior trials, the S_C architecture in Stage 3 continues to demonstrate exceptional performance across the majority of datasets. Upon comparing the experimental results in Tab. 1 (15 minutes to 5 minutes, 3x upsampling) 2 and Tab. 4 (1 hour to 15 minutes, 4x upsampling) 3, we observed a significant phenomenon: as the upsampling factor increases, the reconstruction error of all methods tends to rise. Taking the WPUQ dataset train set as an example, in the 3x upsampling task (Tab. 1), the RMSE of the S_C method is 0.1360; while in the 4x upsampling task (Tab. 4), the RMSE of the same model rises to 0.2051. This performance degradation is prevalent across all comparative models. This phenomenon reveals a fundamental physical limitation in time-series super-resolution tasks: as the temporal granularity of the input data coarsens, the loss of high-frequency information in the original signal increases exponentially, resulting in a substantial increase in the uncertainty of reconstructing its microstructure. Although our S_C model, thanks to the characteristics of GAN, still outperforms traditional interpolation methods in maintaining structural integrity, the overall increase in error due to high-rate sampling remains unavoidable at this stage in the absence of additional prior knowledge.

4.3 MPC Application Scenario

Modern energy systems incorporating renewable energy, energy storage, and smart grids are highly dynamic. Their operations are influenced by weather fluctuations, user behavior, and the volatility of renewable energy production. This leads to continuous changes in system states and loads. Co-simulation offers a practical framework to capturing these dynamics. It involves coupling models from different domains and timescales to obtain a comprehensive representation of system behavior. Model Predictive Control (MPC) is widely used in such co-simulation frameworks, particularly for

coordinating energy storage systems, as it computes an optimal future control trajectory based on predicted system behavior [38]. In each control step, MPC formulates and solves an optimization problem over a finite prediction horizon based on the current system state, forecasted data, and a system model to obtain the optimal control strategy. It only uses the first control action, and then it repeats the steps in a rolling-horizon manner.

The performance of MPC depends on both model fidelity and the temporal resolution of input data. High-resolution measurements, such as 1-minute data, improve the ability to capture system dynamics and enhance control accuracy. Recent work demonstrates that MPC performance in low-voltage distribution grids is particularly sensitive to prediction horizon length and forecast quality [39]. Similar observations arise in data-driven MPC using high-frequency data, such as the 10-second measurements used for high-energy-consumption systems in [40].

With increasing renewable integration, distribution grid operation becomes more challenging, requiring high-temporal-resolution data to capture their impacts and support informed operational decisions [10]. In contrast, low-resolution data (e.g., hourly measurements) reduce computational effort but fail to represent short-term variability and often lack the sensitivity needed for real-time control [41].

Therefore, high-resolution time-series data are essential for MPC-based refined scheduling or real-time optimization. While such high-resolution measurements are often unavailable in practice, this is often due to sensor limitations, low acquisition frequencies, or storage costs. Additionally, the data originate from external models whose output resolutions do not meet MPC requirements. In these cases, the requirement for high-resolution MPC data can be met by upsampling the existing data.

We base our analysis on the scenario from [42], shown in Fig. 4. It uses the benchmark grid "1-LV-rural1-1-sw" from SimBench [43], and on this basis, four solar generation plants are added to the original grid at nodes 6, 9, 12, and 14, which are equipped with battery storage. These battery storages are controlled using the MPC described in [42]. The distribution grid data has a resolution of 15 minutes, which will be downsampled to 1 hour. Then it will be upsampled again to a 15-minute time series using the method S_C and S+C with Phase 3 described in the present paper.

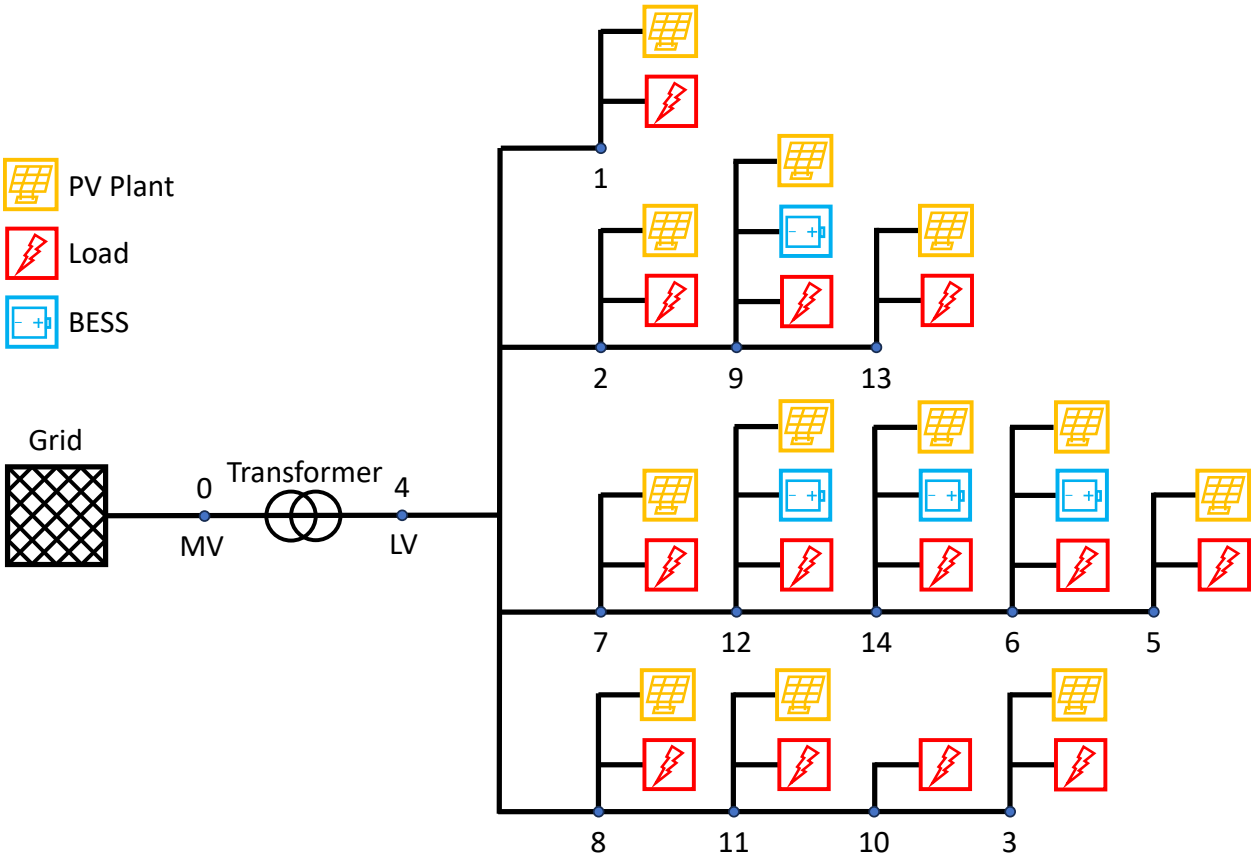

Figure 4: The electrical grid based on [43] and [42] was used as an application scenario.

Table 5: Performance Comparison of Electrical Grid - RMSE and PCC Metrics (lower RMSE and higher PCC indicate better performance)

		L1-A				**L2-A**				**Soil_Alternative_2**				**PV5**	
		P		Q		P		Q		P		Q		pv	
		Train	Test	Train	Test	Train	Test	Train	Test	Train	Test	Train	Test	Train	Test
PCC	Gauss	0.8908	0.8722	0.9274	**0.8850**	0.8987	**0.9041**	0.8785	**0.8817**	0.8930	0.8758	0.8930	0.8758	0.9974	0.9961
	S+C	0.9331	**0.8730**	0.9501	0.8791	0.9434	0.9030	0.9202	0.8734	0.9029	0.8855	0.9029	0.8855	**0.9981**	**0.9968**
	S_C	**0.9504**	0.8692	**0.9706**	0.8763	**0.9567**	0.9023	**0.9487**	0.8678	**0.9100**	**0.8939**	**0.9083**	**0.8927**	0.9975	0.9962
RMSE	Gauss	0.2195	0.2360	0.1864	**0.2320**	0.2175	**0.2147**	0.2322	**0.2297**	0.3117	0.3470	0.3117	0.3470	0.0496	0.0568
	S+C	0.1727	**0.2353**	0.1559	0.2383	0.1652	0.2177	0.1917	0.2405	0.2976	0.3337	0.2976	0.3337	0.0469	0.0544
	S_C	**0.1508**	0.2382	**0.1208**	0.2404	**0.1488**	0.2160	**0.1558**	0.2410	**0.2875**	**0.3227**	**0.2900**	**0.3245**	**0.0328**	**0.0451**
		H0-A				**H0-B**				**H0-C**				**PV6**	
		P		Q		P		Q		P		Q		pv	
		Train	Test	Train	Test	Train	Test	Train	Test	Train	Test	Train	Test	Train	Test
PCC	Gauss	0.8402	**0.8502**	0.5982	0.5911	0.7668	**0.7339**	0.6136	0.6447	0.8145	**0.8567**	0.5856	0.6098	0.9974	0.9961
	S+C	0.9032	0.8425	0.7859	0.6176	0.8735	0.7325	0.7623	**0.6791**	0.8984	0.8427	0.7763	**0.6425**	**0.9986**	**0.9965**
	S_C	**0.9270**	0.8340	**0.8368**	**0.6184**	**0.9115**	0.7262	**0.7965**	0.6734	**0.9316**	0.8361	**0.8238**	0.6425	0.9975	0.9958
RMSE	Gauss	0.2505	**0.2508**	0.3285	0.3010	0.2577	0.2805	0.3179	0.3113	0.2486	**0.2280**	0.3342	0.2999	0.0494	0.0558
	S+C	0.1961	0.2556	0.2393	**0.3010**	0.1928	**0.2759**	0.2476	**0.2839**	0.1882	0.2389	0.2455	**0.2999**	**0.0355**	**0.0523**
	S_C	**0.1735**	0.2602	**0.2125**	0.3011	**0.1644**	0.2788	**0.2314**	0.2866	**0.1585**	0.2442	**0.2215**	0.3065	0.0485	0.0550

In this Section, if the test loss of Phase 3 does not continue to decrease compared to Phase 2, then early stopping will be performed. Tab. 5 shows the results of SR. The best performance for each dataset is highlighted in bold. As shown in the table, the error of S_C on most training datasets, including active power P and reactive power Q, is significantly lower than that of S+C and the Gaussian Process. It is consistent with its ability to fit the training set mentioned above. It is worth reiterating that no high-resolution time series is involved in the training process. However, the fitting performance and generalization performance of S_C on the photovoltaic dataset are not superior to those of S+C. The RMSE values for the PV dataset PV6 are generally much lower than those for the other datasets, which may suggest its inherent smoothness or higher predictability. Nevertheless, minor numerical fluctuations can still lead to large errors.

Table 6: Results of MPC - RMSE and MAE Metrics (lower RMSE and higher PCC indicate better performance)

	RMSE [kW]	MAE [kW]
Gauss	3.0142	1.376
S+C	2.910	1.21
S_C	2.651	1.184

In the presented application scenario, data sampled by different methods are imported into the MPC model. The power curves of the four batteries are calculated. The curves obtained are then compared with the results simulated with real high-resolution data. This is used to evaluate the control error caused by the SR error. Tab. 6 shows the results of MPC simulation. Method S_C maintains its leading position this time. Compared with Gauss Process, S_C has an improvement of $12.05\ \%$ in RMSE and $13.95\ \%$ in MAE.

5 Conclusion and Outlook

To address the data challenges caused by temporal granularity mismatch in energy system co-simulation, this paper proposes a self-supervised super-resolution framework based on a Generative Adversarial Transformer. Existing deep learning super-resolution (SR) or imputation models typically rely on supervised learning, requiring pairs of low-resolution inputs and high-resolution labels (Ground Truth) to compute the loss. However, in real-world upsampling applications, high-resolution data is inherently missing—if high-resolution data existed, upsampling would be unnecessary. The proposed method introduces a Generative Adversarial Network (GAN) structure, utilizing Feature Matching Loss to replace traditional point-to-point error losses (such as MSE). This enables the model to learn the distribution and structural features of data from low-resolution inputs alone, even when real high-resolution samples are unavailable, achieving true self-supervised learning. Without requiring high-resolution data, this method reduces the RMSE by an average of $10\ \%$ on multiple real-world energy datasets and improves the accuracy of a MPC application by $13\ \%$.

Future research will focus more on structural innovation, like compressing three phases into one, and larger-scale experiments are being investigated to verify the statistical reliability of these subtle improvements and improve the model's generalization ability.

Declaration

During the preparation of this work, the authors used Gemini (Google DeepMind) and Claude (Anthropic) in order to perform text polishing and figure creation. After using this tool/service, the author(s) reviewed and edited the content as needed and take full responsibility for the content of the publication.

Acknowledgements

This work is supported in part by the Helmholtz Association through the project "Helmholtz Platform for the Design of Robust Energy Systems and Their Supply Chains" (RESUR), the Helmholtz Energy System Design (ESD) program, and the Helmholtz AI HAICORE partition (HAICORE@KIT).

References

[1] Elisa Papadis and George Tsatsaronis. Challenges in the decarbonization of the energy sector. *Energy*, 205: 118025, 2020. ISSN 0360-5442. doi: https://doi.org/10.1016/j.energy.2020.118025. URL https://www.sciencedirect.com/science/article/pii/S0360544220311324.

[2] Miguel Chang et al. Trends in tools and approaches for modelling the energy transition. *Applied Energy*, 290:116731, 2021. ISSN 0306-2619. doi: https://doi.org/10.1016/j.apenergy.2021.116731. URL https://www.sciencedirect.com/science/article/pii/S0306261921002476.

[3] Karl-Kiên Cao et al. Bridging granularity gaps to decarbonize large-scale energy systems—the case of power system planning. *Energy Science & Engineering*, 9(8):1052–1060, 2021. doi: https://doi.org/10.1002/ese3.891. URL https://scijournals.onlinelibrary.wiley.com/doi/abs/10.1002/ese3.891.

[4] Kris Poncelet et al. Impact of the level of temporal and operational detail in energy-system planning models. *Applied Energy*, 162:631–643, 2016. ISSN 0306-2619. doi: https://doi.org/10.1016/j.apenergy.2015.10.100. URL https://www.sciencedirect.com/science/article/pii/S0306261915013276.

[5] Yusuke Tashiro et al. Csdi: Conditional score-based diffusion models for probabilistic time series imputation. *Advances in neural information processing systems*, 34:24804–24816, 2021.

[6] Georgios Batzolis et al. Conditional image generation with score-based diffusion models, 2021. URL https://arxiv.org/abs/2111.13606.

[7] Mathieu Lepot et al. Interpolation in time series: An introductive overview of existing methods, their performance criteria and uncertainty assessment. *Water*, 9(10), 2017. ISSN 2073-4441. doi: 10.3390/w9100796. URL https://www.mdpi.com/2073-4441/9/10/796.

[8] Mahmoud Nassar et al. Aggregation techniques for time series data: A survey. *Journal of Big Data*, 7(1):1–18, 2020.

[9] Maximilian Hoffmann et al. A review on time series aggregation methods for energy system models. *Energies*, 13 (3), 2020. ISSN 1996-1073. doi: 10.3390/en13030641. URL https://www.mdpi.com/1996-1073/13/3/641.

[10] Olalekan Omoyele et al. Increasing the resolution of solar and wind time series for energy system modeling: A review. *Renewable and Sustainable Energy Reviews*, 189:113792, 2024. ISSN 1364-0321. doi: https://doi.org/10.1016/j.rser.2023.113792. URL https://www.sciencedirect.com/science/article/pii/S1364032123006494.

[11] Zhiguo Cao et al. Learning to upsample by learning to sample. *2023 IEEE/CVF International Conference on Computer Vision (ICCV)*, pages 6004–6014, 2023. doi: 10.1109/ICCV51070.2023.00554.

[12] D. Cohen-Or et al. Pu-net: Point cloud upsampling network. *2018 IEEE/CVF Conference on Computer Vision and Pattern Recognition*, pages 2790–2799, 2018. doi: 10.1109/CVPR.2018.00295.

[13] Jun Han and Chaoli Wang. Tsr-tvd: Temporal super-resolution for time-varying data analysis and visualization. *IEEE Transactions on Visualization and Computer Graphics*, 26:205–215, 2020. doi: 10.1109/TVCG.2019.2934255.

[14] Zhengping Che, Sanjay Purushotham, Kyunghyun Cho, David Sontag, and Yan Liu. Recurrent neural networks for multivariate time series with missing values. *Scientific reports*, 8(1):6085, 2018.

[15] Wei Cao et al. Brits: bidirectional recurrent imputation for time series. In *Proceedings of the 32nd International Conference on Neural Information Processing Systems*, NIPS'18, page 6776–6786, Red Hook, NY, USA, 2018. Curran Associates Inc.

[16] Eoin Brophy et al. Generative adversarial networks in time series: A systematic literature review. *ACM Comput. Surv.*, 55(10), February 2023. ISSN 0360-0300. doi: 10.1145/3559540. URL https://doi.org/10.1145/3559540.

[17] Ian Goodfellow et al. Generative adversarial networks. *Commun. ACM*, 63(11):139–144, October 2020. ISSN 0001-0782. doi: 10.1145/3422622. URL https://doi.org/10.1145/3422622.

[18] Rui Tang et al. Interpolating high granularity solar generation and load consumption data using super resolution generative adversarial network. *Applied Energy*, 299:117297, 2021. ISSN 0306-2619. doi: https://doi.org/10.1016/j.apenergy.2021.117297. URL https://www.sciencedirect.com/science/article/pii/S0306261921007108.

[19] Jinsung Yoon et al. Time-series generative adversarial networks. In H. Wallach, H. Larochelle, A. Beygelzimer, F. d'Alché-Buc, E. Fox, and R. Garnett, editors, *Advances in Neural Information Processing Systems*, volume 32. Curran Associates, Inc., 2019.

[20] Abdellah Madane et al. Transformer-based conditional generative adversarial network for multivariate time series generation, 2022. URL https://arxiv.org/abs/2210.02089.

[21] Gökhan Demirel et al. Synthesizing Distribution Grid Congestion Data Using Multivariate Conditional Time Series Generative Adversarial Networks. In *2024 IEEE iSPEC*, pages 385–390, 2024. doi: 10.1109/iSPEC59716.2024.10892479.

[22] Yifan Xu et al. Transformers in computational visual media: A survey. *Computational Visual Media*, 8:33–62, 2022. doi: 10.1007/s41095-021-0247-3.

[23] Yuxuan Wang et al. Deep Time Series Models: A Comprehensive Survey and Benchmark, 2024. URL https://arxiv.org/abs/2407.13278.

[24] Shizhan Liu et al. Pyraformer: Low-complexity pyramidal attention for long-range time series modeling and forecasting. In *International Conference on Learning Representations*, 2022. doi: 10.34726/2945. URL https://openreview.net/forum?id=0EXmFzUn5I.

[25] Tian Zhou et al. Fedformer: Frequency enhanced decomposed transformer for long-term series forecasting. In *International conference on machine learning*, pages 27268–27286, Baltimore, MD, USA, 2022. PMLR.

[26] Shengnan Guo et al. Learning dynamics and heterogeneity of spatial-temporal graph data for traffic forecasting. *IEEE Transactions on Knowledge and Data Engineering*, 34(11):5415–5428, 2022. doi: 10.1109/TKDE.2021.3056502.

[27] Mushui Liu et al. CM-UNet: Hybrid CNN-Mamba UNet for Remote Sensing Image Semantic Segmentation, 2024. URL https://arxiv.org/abs/2405.10530.

[28] Xiaomin Li et al. Tts-gan: A transformer-based time-series generative adversarial network, 2022. URL https://arxiv.org/abs/2202.02691.

[29] Richard Zhang et al. The unreasonable effectiveness of deep features as a perceptual metric. In *Proceedings of the IEEE conference on computer vision and pattern recognition*, pages 586–595, 2018.

[30] Tim Salimans et al. Improved techniques for training gans. In *Proceedings of the 30th International Conference on Neural Information Processing Systems*, NIPS'16, page 2234–2242, Red Hook, NY, USA, 2016. Curran Associates Inc. ISBN 9781510838819.

[31] Alex Kendall et al. Multi-task learning using uncertainty to weigh losses for scene geometry and semantics. In *Proceedings of the IEEE Conference on Computer Vision and Pattern Recognition*, pages 7482–7491, 2018.

[32] Ian J. Goodfellow et al. Generative adversarial nets, 2014. URL https://arxiv.org/abs/1406.2661.

[33] Marlon Schlemminger et al. Dataset on electrical single-family house and heat pump load profiles in germany. *Scientific data*, 9(1):56, 2022.

[34] A Dittmann et al. PV-Live dataset - Measurements of global horizontal and tilted solar irradiance, 2022.

[35] Daniel Vázquez Pombo et al. Multi-Horizon Data-Driven Wind Power Forecast: From Nowcast to 2 Days-Ahead. In *2021 International Conference on Smart Energy Systems and Technologies (SEST)*, pages 1–6, 2021. doi: 10.1109/SEST50973.2021.9543173.

[36] Gökhan Demirel et al. PIDE: Photovoltaic integration dynamics and efficiency for autonomous control on power distribution grids. *Energy Informatics*, 8(1):32, 2025. ISSN 2520-8942.

[37] Christian Ledig, Lucas Theis, Ferenc Huszar, Jose Caballero, Andrew Cunningham, Alejandro Acosta, Andrew Aitken, Alykhan Tejani, Johannes Totz, Zehan Wang, and Wenzhe Shi. Photo-Realistic Single Image Super-Resolution Using a Generative Adversarial Network . In *2017 IEEE Conference on Computer Vision and*

Pattern Recognition (CVPR), pages 105–114, Los Alamitos, CA, USA, July 2017. IEEE Computer Society. doi: 10.1109/CVPR.2017.19. URL `https://doi.ieeecomputersociety.org/10.1109/CVPR.2017.19`.

[38] Diego I. Hidalgo-Rodríguez and Johanna Myrzik. Optimal operation of interconnected home-microgrids with flexible thermal loads: A comparison of decentralized, centralized, and hierarchical-distributed model predictive control. In *2018 PSCC*, pages 1–7, 2018. doi: 10.23919/PSCC.2018.8442807.

[39] Gökhan Demirel et al. Linear and Nonlinear Model Predictive Control for Distributed Energy Resources in Power Grids. In *2025 IEEE 13th SEGE*, pages 213–219, 2025. doi: 10.1109/SEGE65970.2025.11203658.

[40] Jiawei Chen et al. Data-driven learning-based model predictive control for energy-intensive systems. *Advanced Engineering Informatics*, 58:102208, 2023.

[41] Stefan Pfenninger. Dealing with multiple decades of hourly wind and pv time series in energy models: A comparison of methods to reduce time resolution and the planning implications of inter-annual variability. *Applied energy*, 197:1–13, 2017.

[42] Felicitas Mueller et al. Sector-coupled distribution grid analysis for centralized and decentralized energy optimization. In *2023 58th International UPEC*, pages 1–6. IEEE, 2023.

[43] Steffen Meinecke et al. Simbench—a benchmark dataset of electric power systems to compare innovative solutions based on power flow analysis. *Energies*, 13(12), 2020. ISSN 1996-1073.

[44] E. Hewitt and R. E. Hewitt. The gibbs-wilbraham phenomenon: An episode in fourier analysis. *Archive for History of Exact Sciences*, 21(2):129–160, 1979.

A Baseline Selection

This section employs Long Short-Term Memory (LSTM), Temporal Convolutional Network (TCN), and TF as baseline models, which exemplify three fundamental and significant methodologies in time series analysis [23]. LSTM, as a prototypical recurrent neural network (RNN), is a well-established architecture designed for sequence data processing and is widely used in time series research. TCN denotes the utilization of convolutional neural networks (CNN), which excel at identifying local features and patterns in data via convolutional operations. The TF, utilizing its robust self-attention mechanism, has exhibited exceptional proficiency in capturing long-term temporal dependencies and intricate connections, establishing itself as a sophisticated backbone architecture. To evaluate the performance of the candidate architectures presented above, a series of controlled experiments for interpolation on a variety of waveform tasks are introduced, including simple linear trends, square waves with mutations, smooth sinusoids, and sawtooth patterns exhibiting discontinuities. All networks use the most basic structure. Fig. 5 shows the results of three models in

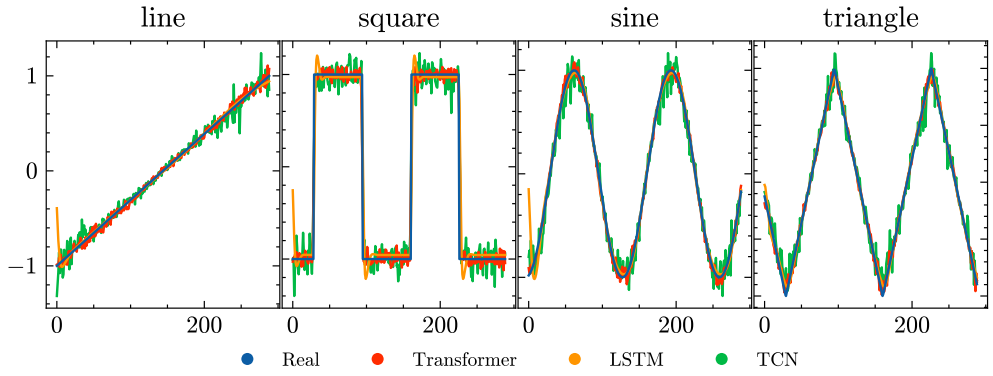

Figure 5: Baseline Selection.

four types of waveform interpolation tasks. In the linear waveform task, whereas LSTM is closer to the real trend line, TF TCN has prominent oscillations. The square wave task best reflects the difference between the models. TF captures the jump transition. However, LSTM has a smoothing phenomenon at the transition point and cannot maintain sharp edges, and produces the Gibbs phenomenon [44]. TCN still maintains severe oscillations. In the triangle wave test, TF and LSTM can maintain the sharp peak characteristics well, but only exhibit a certain degree of smoothing effect, resulting in rounded peaks. TCN exhibits the most severe oscillation in all tasks. However, LSTM has a significant error at the beginning of the output due to limited context. That is, the model based on the RNN structure can only see

information from the past. This causes the model to show significant deviations at key points of the resampled signal (such as the beginning or step of the sequence). Overall, TF has advantages in processing various complex waveforms, especially those containing discontinuities.

Table 7: Performance Metrics Comparison

Metric	Model	Line	Square	Sine	Triangle
RMSE	TCN	0.0758	0.2049	0.1012	0.0857
	LSTM	0.0491	0.2090	0.0599	0.0515
	TF	**0.0356**	**0.1721**	**0.0403**	**0.0359**
MAE	TCN	0.0528	0.1167	0.0761	0.0644
	LSTM	**0.0160**	0.0839	**0.0274**	**0.0255**
	TF	0.0272	**0.0659**	0.0311	0.0271
PCC	TCN	0.9914	0.9788	0.9898	0.9890
	LSTM	0.9964	0.9781	0.9965	0.9960
	TF	**0.9981**	**0.9851**	**0.9984**	**0.9981**

Tab. 7 presents an analysis of the performance of three models across four distinct waveform resampling tasks, utilizing Root Mean Square Error (RMSE), Mean Absolute Error (MAE), and Pearson Correlation Coefficient (PCC) as evaluative metrics. The TF performs best in all four tasks, achieving the lowest RMSE and the highest PCC. The TCN model has the highest overall error rate in all tests and its performance is relatively weakest among the three. It is worth noting that the square wave task poses the most severe challenge to all models. In summary, both qualitative (Fig. 5) and quantitative (Tab. 7) evidence suggests that it is reasonable to choose TF as the baseline model for this article.

B Feature Fusion

In the present paper, the feature fusion layer we used, as shown in Fig. 6, is based on a multi-scale attention aggregation (MSAA) module [27]. This feature fusion layer receives outputs from multiple attention mechanisms. It performs feature extraction and aggregation using the spatial attention mechanism on the left and the channel attention mechanism on the right. Finally, the results are fused through addition and 1D convolution.

Features from multiple attention mechanisms $X_1 \in \mathbb{R}^{C\times H\times W}$, $X_2 \in \mathbb{R}^{C\times H\times W}$,..., $X_N \in \mathbb{R}^{C\times H\times W}$ are spliced on the channel and then downscaled by 1-dimensional convolution, where the number of channels after convolution D is less than the number of channels before convolution C:

$$X \in \mathbb{R}^{D\times H\times W} = \text{Conv}(\text{Concat}(X_1, X_2, X_3)) \tag{10}$$

In the spatial attention mechanism, multi-scale fusion is achieved by concatenating and summing X through multiple convolutional layers with different convolutional kernel sizes:

$$X_1 \in \mathbb{R}^{D\times H\times W} = \text{Conv}_{3\times 3}(X) \tag{11}$$

$$X_2 \in \mathbb{R}^{D\times H\times W} = \text{Conv}_{5\times 5}(X) \tag{12}$$

$$X_3 \in \mathbb{R}^{D\times H\times W} = \text{Conv}_{7\times 7}(X) \tag{13}$$

$$S \in \mathbb{R}^{D\times H\times W} = X_1 + X_2 + X_3 \tag{14}$$

The output of the multi-scale fusion fed to average pooling and maximum pooling in the channel domain, followed by concatenation. It is then downscaled using a 1D convolution and generates spatial feature weights through sigmoid functions:

$$W_s \in \mathbb{R}^{1\times H\times W} = \text{Sigmoid}(\text{Conv}(\text{Pool}(S))) \tag{15}$$

The generated spatial feature weights W_s are then used to adjust the inputs to get the final spatial feature output:

$$O_s \in \mathbb{R}^{D\times H\times W} = W_s U \tag{16}$$

The channel attention on the right is used to adjust the channel weights of the input features. Given the input $X \in \mathbb{R}^{D\times H\times W}$, first the mean and maximum pooling in the spatial domain are performed to obtain the channel features respectively. The correlation between the channels is learned by two 1D convolutions and the channel weight representation is generated by the sigmoid function:

$$W_c \in \mathbb{R}^{D\times 1\times 1} = \text{Sigmoid}(\text{Conv}(\text{Conv}(\text{Pool}(X)))) \tag{17}$$

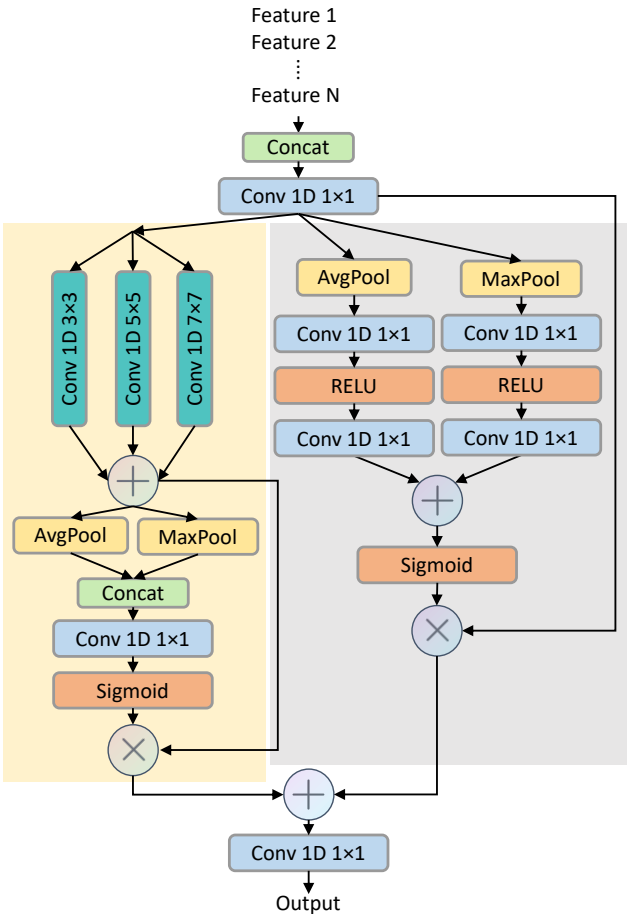

Figure 6: Feature Fusion.

The generated channel feature weights W_c are then used to adjust the inputs to get the final channel feature output:

$$O_c \in \mathbb{R}^{D\times H\times W} = W_c X \tag{18}$$

The final channel feature output and the final channel feature output are summed and recovered by a 1D convolutional layer with the same number of channels as the input:

$$O \in \mathbb{R}^{C\times H\times W} = \text{Conv}(O_s + O_c) \tag{19}$$

The result is the fused feature.